Processing and Mechanical Properties of Al_2O_3 Fiber-Reinforced NiAl Composites

R.R. BOWMAN, A.K. MISRA, and S.M. ARNOLD

The mechanical properties of NiAl-matrix composites reinforced with 125-μm diameter single-crystal Al_2O_3 (sapphire) fibers have been examined over the temperature range of 300 to 1200 K. Composites were fabricated with either a strong or weak fiber-matrix interfacial bond strength. During fabrication, a fiber-matrix interaction occurred such that fibers extracted from the NiAl matrix were fragmented and significantly weaker than the as-received fibers. Tensile results of the weakly bonded composite demonstrated that the composite stiffness was greater than the monolithic at both 300 and 1200 K in spite of the weak bond. Room-temperature strengths of the composite were greater than that of the monolithic but below rule-of-mixture predictions (even when the degraded fiber strengths were accounted for). At 1200 K, the ultimate strength of the composite was inferior to that of the monolithic primarily because of the poor fiber properties. No tensile data was obtained on the strongly bonded material because of the occurrence of matrix cracking during fabrication. Primarily because of the fiber strength loss, sapphire-NiAl composite mechanical properties are inferior to conventional high-temperature materials such as superalloys and are currently unsuitable for structural applications.

I. INTRODUCTION

In recent years, vast resources have been directed toward the development of structural materials with use temperatures significantly above those of current generation superalloys. Gradual evolution of proven materials is a low-risk approach for achieving increased material performance but offers only limited improvements in temperature capabilities. Conversely, while the low density and high melting temperatures of intermetallic compounds offer substantially higher use temperatures, development of these systems presents a proportionally greater challenge. Of the numerous intermetallics under consideration, NiAl is especially attractive because of its combination of low density (5.9 g/cm^3), high melting temperature (1910 K), high thermal conductivity, and excellent oxidation resistance.[1]

Although the potential of NiAl is intriguing, its viability is in doubt because of its low elevated-temperature strength and poor ambient-temperature toughness. While microalloying has proven successful in improving high-temperature properties, these improvements have been possible only at the expense of toughness.[2] Similarly, increased low-temperature toughness has been achieved only with a concomitant decrease in flow strength. An alternative approach for increasing both strength and damage tolerance is through the use of composites. Most NiAl composites investigated thus far can be categorized as follows: (1) *in situ* composites containing a continuous, ductile, second phase, such as Ni_3Al,[3] Mo,[4] or Cr;[5] (2) discontinuously reinforced composites, where the NiAl matrix is strengthened by a fine dispersion of either particulates (such as TiB_2,[6] AlN,[7] or ZrO_2[8]) or Al_2O_3 whiskers;[9] and (3) continuous-fiber-reinforced NiAl.[10-13] One impetus for the current study has been the interest in continuous-fiber reinforced NiAl as a potential material for the High-Speed Civil Transport (HSCT) program.[14]

Any potential reinforcing fiber must possess high-temperature strength and be compatible with the matrix. The compatibility requirement refers to both mechanical as well as chemical compatibility. Mechanical compatibility is achieved by having similar coefficients of thermal expansion (CTE), thereby minimizing thermally generated stresses in both the matrix and fiber. Elimination of these stresses is of paramount importance in NiAl-base systems ($CTE_{1200\,K} = 15 \times 10^{-6}/K$[15]) because of NiAl's low fracture toughness (~5 MPa$\sqrt{m}$[16]) and limited failure strain. Chemical compatibility is required for long-term stability of the composite system under a variety of thermal histories and environments. Additionally, the fiber must be readily available in quantities sufficient for developmental studies. At present, single crystal Al_2O_3 ($CTE_{1200\,K} = 11 \times 10^{-6}/K$[17]) has the greatest prospect for meeting these requirements.

Alumina fibers have long been recognized as potential reinforcements for high-temperature Ni-base (Ni alloys and superalloys) composites due to their high modulus and strength, low density, and chemical stability. In early studies, concerns about fiber reactions, CTE mismatch, fiber-matrix bonding, and high cost resulted in pessimistic views about the prospects of ceramic whiskers or fibers as a reinforcement in metal matrix composites.[18] It soon became apparent that the strength of sapphire could be severely degraded by reaction with the matrix. This reaction led to fiber fragmentation during processing and poor composite properties. While a strong bond is desirable for composite strengthening, especially during transverse loading, numerous studies have shown that there is an inherent relationship between increased bond strength, chemical reaction at the interface, and decrease in fiber strength. The conclusion from early studies was that diffusion-barrier coatings would be necessary for Al_2O_3 reinforced Ni- and superalloy-base composites.

R.R. BOWMAN and S.M. ARNOLD, Research Engineers, are with the NASA Lewis Research Center, Cleveland, OH 44135. A.K. MISRA, Research Engineer, is with NYMA Inc., LeRC Group, Brookpart, OH 44142.

Manuscript submitted March 17, 1994.

It is as yet unclear to what degree interfacial control, such as through the use of fiber coatings, will be required to realize the full potential of Al_2O_3/NiAl. Recent analytical modeling has suggested that a compliant or compensating fiber coating may be necessary to reduce the tendency for matrix cracking due to thermally generated stresses. However, NiAl is predicted to be chemically compatible with Al_2O_3, from both thermodynamic calculations[19] and from preliminary experimental results.[11] Before a systematic study of fiber coatings should be undertaken, it must be clearly understood what effect a weak vs strong interfacial bond, in the absence of an interfacial phase or coating, has on composite properties. It is also necessary to examine fiber reaction and its effect on fiber strength and composite properties in an NiAl matrix composite. Only then can the characteristics of the interface be prescribed and perhaps tailored by the use of coatings for specific requirements.

II. EXPERIMENTAL PROCEDURES

All composites in this study were fabricated from 50 to 150-μm diameter vacuum-atomized, prealloyed, stoichiometric NiAl powders (Table I) obtained from Homogeneous Metals, Inc. (Clayville, NY). The composites were reinforced with continuous, uncoated (no protective sizing), 125-μm diameter, c-axis-oriented, single-crystal Al_2O_3 fibers supplied by Saphikon, Inc. (Milford, CT). Most of the composites were fabricated using the powder-cloth (PC) technique.[20] In this process, the matrix material was processed into flexible clothlike sheets by combining matrix powders with poly(tetrafluoroethylene) (TEFLON*). Likewise, fiber mats were produced by winding the fibers at a spacing of 40 fibers/cm on a drum and applying another organic binder, poly(methyl methacrylate) (PMMA). The composite panel was assembled by stacking alternate layers of matrix cloth and fiber mats. This assemblage was hot-pressed, during which the fugitive binders were volatilized and the composite was consolidated to near full density. This was followed by hot isostatic pressing ("hiping") to ensure complete densification of the composite. After hiping, the steel containment can and Mo cladding, required in the consolidation process, were removed by chemical etching in a bath of 45 pct nitric acid, 45 pct water, and 10 pct sulfuric acid. The resulting composite plates measured 15 cm long by 5 cm wide and 0.3 cm thick, with 6 plies of fibers comprising a total of about 25 volume fraction (V_f) of the composite. As an alternative to the PC technique, composite plates were fabricated without the use of fugitive binders by directly hot-pressing fibers in a die of matrix powders, followed by hiping. A disadvantage of the binderless technique is that it is more labor intensive and the maximum fiber volume fraction possible is only about 10 pct. Because fibers are manually placed in the powder die, the fiber distribution is less uniform and fiber alignment is poorer than is achieved by winding.

*TEFLON is a trademark of E.I. DuPont de Nemours and Co., Inc., Wilmington, DE.

Table I. Chemical Composition of NiAl Starting Powders and Composite Matrices (At. Pct)

	Ni	Al	C	O	N
Starting powders	50.3	49.7	0.011	0.046	0.006
Powder cloth	50.2	49.8	0.101	0.211	0.005
Binderless	50.1	49.8	0.023	0.073	0.005

Composite properties reported here are from specimens fabricated over several months. Fibers used in the fabrication of the composite specimens came from various spools grown over a similar time frame. To account for differences in composite properties that may have resulted from different as-received fiber strengths, fiber tensile properties were measured on samples taken from each fiber mat used for composite fabrication. To assess the effect of processing on the fiber strengths, fibers were etched from the composites using a bath of 50 pct water, 33 pct nitric acid, and 17 pct hydrochloric acid at 345 K. Complete dissolution of the matrix typically required 3 hours. Tensile properties of as-received and extracted fibers were measured at 300 and 1200 K. Some as-received fibers were also exposed to the acid bath and subsequently tested to insure that the chemical bath itself did not affect fiber strengths. Fiber tensile testing was performed under displacement-controlled conditions with a crosshead speed of 0.127 cm/min. The room-temperature gage length (grip distance) was 1.27 cm. Longer specimens were needed for high-temperature testing to accommodate the furnace. For these tests, although the grip distance was 15 cm, the hot zone of the furnace was measured to be 1.27 cm and was assumed to be the fiber gage length.

The properties of the matrix material were evaluated by hot pressing and hiping NiAl powders and testing the resultant monolithic material in the same fashion as that used for the composites described subsequently. Because of NiAl's extreme sensitivity to composition and cleanliness,[11] mechanical property variations existed between individual lots of powder. Small deviations in stoichiometry or the presence of impurities, such as carbon at levels as low as 500 ppm, can dramatically raise the yield and flow stress and result in increased brittleness. For consistency, all properties reported here are from composites fabricated from a single batch of powder. The chemical composition of the starting powders are given in Table I along with the composition of the NiAl matrix from composites fabricated by the PC and binderless techniques.

Fiber-matrix interfacial shear stresses were measured at 300 K using techniques described in detail elsewhere.[21] The specimens were typically cut and polished down to 350 to 500-μm thick perpendicular to the fiber direction. Individual fibers were positioned over a 800-μm-wide groove to allow for unconstrained pushout. Pushout was accomplished using a 125-μm-diameter indentor with a flat-bottom geometry at a crosshead speed of 10 μm/s. In each case, a load-displacement curve was generated during fiber pushout, from which both the debond and frictional component of the interfacial strength could be determined.

Tensile specimens were waterjet machined from the

Table II. Material Properties Used in Residual-Stress Calculations

Property	Units	NiAl	Al_2O_3
Yield stress	MPa	$167 - 0.08\ (T)$	—
Elastic modulus	GPa	$204.9 - 0.041\ (T)$	$463.6 - 0.040\ (T)$
Shear modulus	GPa	$76.6 - 0.017\ (T)$	146
Poission's ratio		$0.307 + 2.15 \times 10^{-5}\ (T)$	0.30
Thermal expansion	K^{-1}	$1.16026 \times 10^{-5} + 4.08531 \times 10^{-9}\ (T) - 1.58368 \times 10^{-12}\ (T)^2 + 4.18374 \times 10^{-16}\ (T^3)$	$5.932 + 0.425 \times 10^{-2}\ (T) - 0.634 \times 10^{-6}\ (T^2) - 0.7017 \times 10^{-11}\ (T^3)$

as-fabricated plates and any surface irregularities removed with 180-grit SiC paper before testing. Composite tensile specimens were machined with the fibers oriented parallel to the loading direction and with reduced gage dimensions of 1.524-cm long by 0.635-cm wide. Tensile tests were performed at 300 and 1200 K in air under displacement-controlled conditions with a cross-head speed of 0.0127 cm/min. Strain was measured on all tensile specimens using a 1.27-cm gage length extensometer. The resultant nominal strain rate was 1.7×10^{-4}/s. All high-temperature testing was performed in a resistance furnace with a temperature gradient in the gage section of no more than ±5 K. Specimen gripping was achieved using water-cooled hydraulic grips with a 225-kg load. For the high-temperature tests, the specimens were held at temperature for 30 minutes before testing. At least three duplicate tests were performed for each condition. Tests were both conducted to failure as well as interrupted at various strain levels for microscopic examination of the failure process. Acoustic emission (AE) data were collected during the room-temperature tests to assist in identifying the failure mechanism. The AE sensors were attached at both ends of the gage section and recorded the location along the gage length of each AE event.

III. RESULTS

A. *Interfacial Bond Strength*

Load-displacement curves were used to determine the debond and frictional components of bond strength for PC and binderless processed composites. The maximum load obtained during pushout was used to calculate the debonding stress (τ_d); the load required for subsequent fiber pushout is associated with the frictional component (τ_f) of the bond strength. Composites fabricated by the PC technique had room-temperature interfacial debonding strengths of 102.8 ± 23.2 MPa with a frictional bond of 40.1 ± 3.6 MPa. Composites that were fabricated with binders only on the fibers (PMMA) or only in the powders (TEFLON) had similarly low bond strengths. Longer hold times in the hot press, to allow for more complete volatilization of the binders, also had no effect on bond strength. In contrast to the composites fabricated with binders, the room-temperature interfacial debonding strengths for the binderless processed composites were in excess of 280 MPa. Only a lower limit is estimated for the binderless materials because, in most instances, either the matrix, fiber, or indentor cracked prior to achieving fiber pushout. However, in a small number of tests, the binderless processed fibers could be pushed out. In those cases where fiber pushout was possible, a distinct load drop occurred and was followed by stable pushout with a frictional load similar to the PC processed composites. For subsequent discussions, where distinguishing between bond strength will enhance clarity, PC processed composites alternatively will be referred to as weakly bonded composites and the binderless material as strongly bonded composites.

B. *As-Fabricated Microstructures*

Figure 1 shows transverse optical micrographs of as-fabricated Al_2O_3/NiAl processed by (a) the PC and (b) binderless techniques. The disadvantage of the binderless process is evident in these micrographs, where a less uniform spacing and lower V_f of fibers is observed in Figure 1(b). The fiber V_f in PC processed materials was very reproducible and averaged 25 ± 3 pct. In the binderless technique, fibers were individually placed in a powder die and therefore a maximum V_f of only about 10 pct, with 3 fiber plies, was possible. Although variability of V_f is possible in the binderless technique, only those specimens that contained approximately 10 pct fibers were included in this study. Because of process variability, complete densification of the composite is not assured by either technique. For the purposes of this study, the as-fabricated composites were screened and only plates where full densification occurred, such as the one shown in Figure 1, were included. Both processes produced a matrix material with equiaxed 30-μm grains. No fiber-matrix interfacial reaction products were observed by scanning electron microscopy (SEM). Both processes produced continuous fiber-matrix interfacial regions with no evidence of debonding.

No matrix cracks were observed in the as-fabricated, weakly bonded composites. Conversely, while no radial or tangential matrix cracks were present in the strongly bonded composites, extensive transverse (perpendicular to the fiber direction) cracking of the matrix did occur. These cracks were not present immediately after fabrication; rather, they formed during water-jet machining of the 15-cm tensile specimens. A total of eight fully consolidated plates containing ~10 V_f of strongly bonded fibers were fabricated by the binderless technique with no evidence of matrix cracking. However, in all cases, transverse cracking *was* observed in tensile specimens machined from these plates with a fairly consistent crack spacing of about 0.5 cm. A slight curvature in the thickness direction was also noted in the specimens after machining.

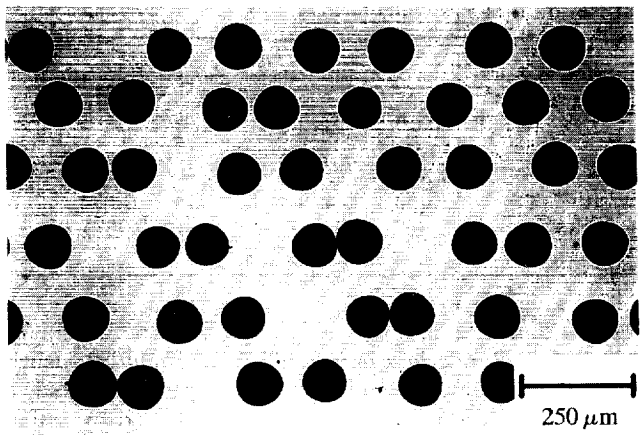

(a)

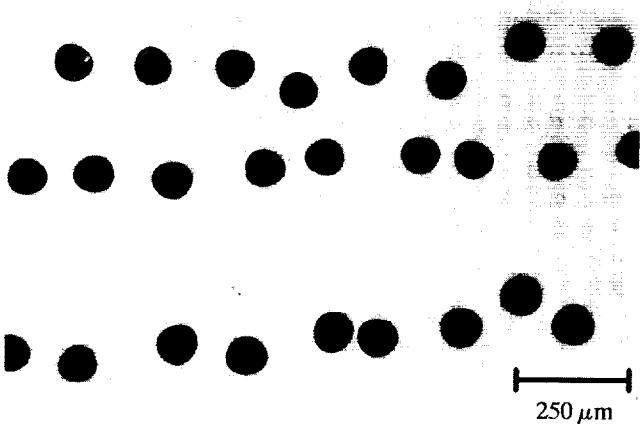

(b)

Fig. 1—Transverse optical micrographs of Al_2O_3/NiAl composites fabricated by the (*a*) PC and (*b*) binderless techniques. Binderless composites have a lower volume fraction of fibers and a less uniform fiber distribution, along with stronger fiber-matrix interfacial bond strengths.

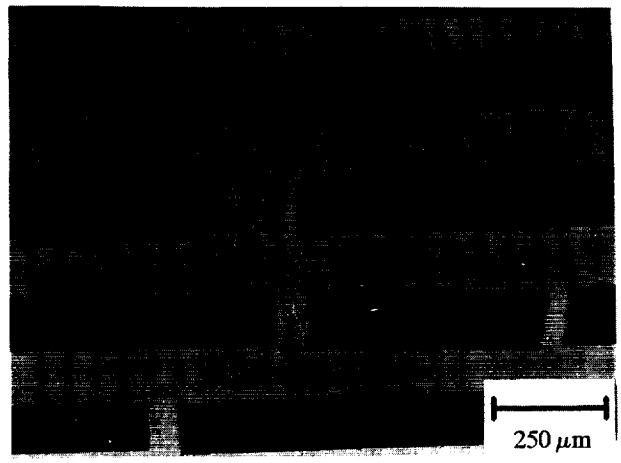

(a)

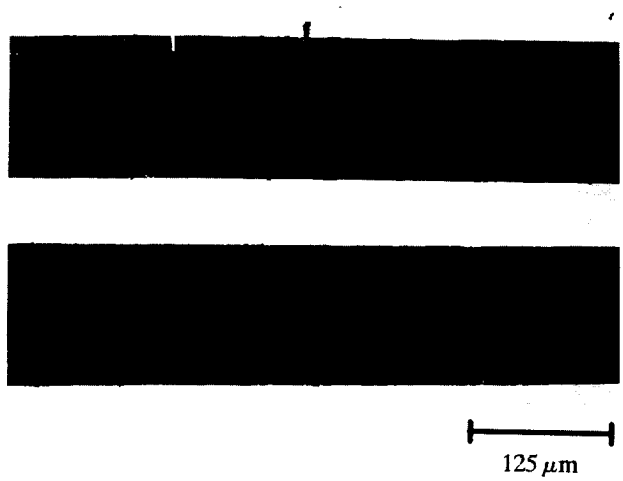

(b)

Fig. 2—Optical micrographs of as-fabricated Al_2O_3/NiAl composite fabricated by the PC technique. Two types of fiber failures were noted. In (*a*), the fractured fiber ends have separated allowing for matrix infiltration. In (*b*), another area of the same composite contains fibers where no matrix infiltration is noted.

Examinations of polished longitudinal sections revealed two types of as-fabricated fiber fractures in both the strongly and weakly bonded composites. In one failure mode, shown in Figure 2(a), the fiber has fractured and the ends separated; matrix material subsequently infiltrated between the broken ends. On the other hand, instances of fiber failures were also observed where the fractured surfaces did not separate and hence no matrix infiltration was noted (Figure 2(b)). Both types of cracks were observed in approximately equal proportions throughout the as-fabricated plates. Metallographic examination and X-ray techniques were incapable of unambiguously determining whether fiber cracking was uniformly distributed throughout the plates or localized in a particular region.

C. *Fiber Properties*

For both the PC and binderless processed composites the average extracted fiber length was substantially less than the original 15 cm, which is consistent with the metallographic observations of fractured fibers (Section III–B). The extent of fragmentation is quantified in Figure 3, where a typical extracted fiber size distribution from a PC processed composite is presented. In Figure 3, for example, 17 pct of the fibers extracted from the 15-cm plate were in the 0 to 1-cm range, while only 2 pct were longer than 12 cm. As seen in this graph, no full-length fibers (0 pct in the 14 to 15-cm range) were observed. Fibers extracted from composites fabricated without binders had a similar distribution of fiber lengths.

Room-temperature and 1200-K as-received and extracted fiber fracture strengths (σ_f^*) are presented in Figure 4, using a two-parameter Weibull[22] distribution. Weibull techniques are commonly used for materials in which failure is controlled by a "weakest link" criteria. For such materials, a linear relationship exists when ln (ln $(1/(1 - P))$ is plotted *vs* $\ln(\sigma_f^*)$. The term P is a

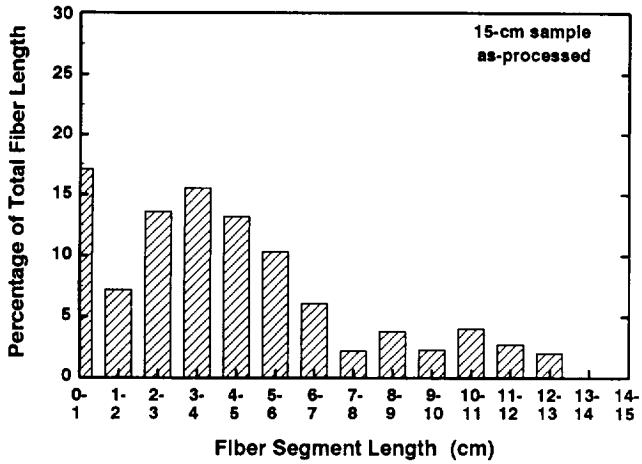

Fig. 3—Length distribution of fibers extracted from an as-fabricated PC processed Al_2O_3/NiAl composite. Fiber fragmentation occurred during processing such that all fiber lengths were less than the original 15 cm.

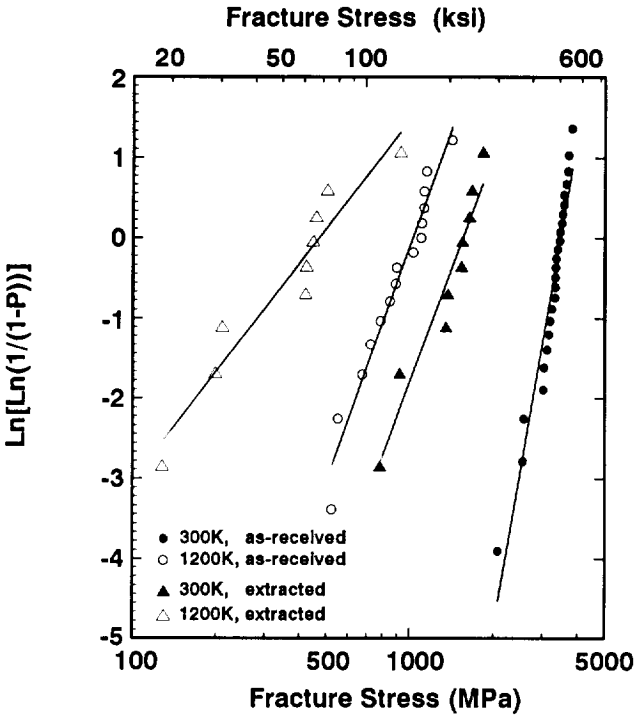

Fig. 4—Room temperature and 1200 K tensile strengths of as-received and extracted Al_2O_3 fibers. Both PC and binderless composite processing techniques resulted in similar fiber strength degradation.

cumulative probability function, which represents the probability of failure at or below some stress σ. The most appropriate form for P has been the subject of both theoretical[23] and experimental[24] investigation. In both of the previously cited studies, the most appropriate form was found to be $P_i = (i - 0.5)/N$, where i is the ith result of a set of ranked fracture stress values, and N is the total number of tests. The slope of the regression line is the Weibull modulus (m). While m cannot be correlated to a particular material property,[25] it does describe the defect population present in the fibers. It was found that the strength distributions of fibers from the various spools used in this study were indistinguishable from each other. Thus, any differences in composite properties cannot be attributed to different fiber lots.

The strong temperature dependence of fracture stress in Al_2O_3 fibers is evident when comparing as-received strengths at 300 K to those at 1200 K (Figure 4). A decrease in strength from room-temperature properties of approximately 65 pct is observed at 1200 K. In addition to temperature-induced strength loss, fiber strength loss resulting from processing is also evident in Figure 4. A strength reduction of approximately 50 pct is observed in fibers extracted from composites fabricated by either the P-C or binderless (not included in Figure 4) techniques as compared to as-received strengths. This processing-induced strength degradation is observed at both 300 and 1200 K. Also, the strengths of fibers extracted from PC processed composites shown in Figure 4 were nearly identical to those extracted from the binderless composites. These results are consistent with those of Draper and Locci,[26] who observed fiber strength reduction in Al_2O_3 fibers etched from PC processed NiAl, FeAl + B, and FeCrAlY. The SEM examination of the extracted fibers revealed the presence of surface ridges, corresponding to the NiAl matrix grain boundaries, on both PC and binderless processed fibers. Such ridging has been noted previously in Al_2O_3/Ni alloy[27] and Al_2O_3/NiAl[28] composites and in Al_2O_3/Nb diffusion couples.[29] Although localized surface attack was observed in the form of ridging, no generalized surface roughening, which has often been reported when chemical bonding of Al_2O_3 to metals occurs, was observed on either the strongly or weakly bonded fibers. Fibers extracted from PC processed material often had C-rich areas on the fiber surface. No correlation was observed between the amount or the location of the C-rich areas and the ridging. These C-rich areas are residue left from incomplete volatilization of the binder materials. It has been suggested[30] that these deposits may act as fracture-initiation sites and thus can be detrimental to fiber strength.

D. *Tensile Properties*

Room-temperature and 1200-K tensile properties of monolithic NiAl and the weakly bonded Al_2O_3/NiAl composites are discussed subsequently. No tensile data could be obtained for the strongly bonded composites because of the formation of through-thickness, transverse cracks during machining of the tensile specimens (Section III–B).

1. *Monolithic NiAl*

A typical tensile curve for monolithic NiAl at 300 and 1200 K is shown in Figures 5(a) and (b) respectively. The NiAl matrix material had a room-temperature elastic modulus of 241 ± 15 GPa and a yield stress of 120 ± 15 MPa with an elastic strain of 0.05 pct. The total strain to failure for all tests was 0.4 ± 0.05 pct. Moderate work hardening was observed after yielding until failure. A yield strength of 120 MPa is relatively low compared to most published data on polycrystalline NiAl, in which a yield stress of 300 MPa is typical with nearly zero tensile ductility. Due to small differences in both stoichiometry

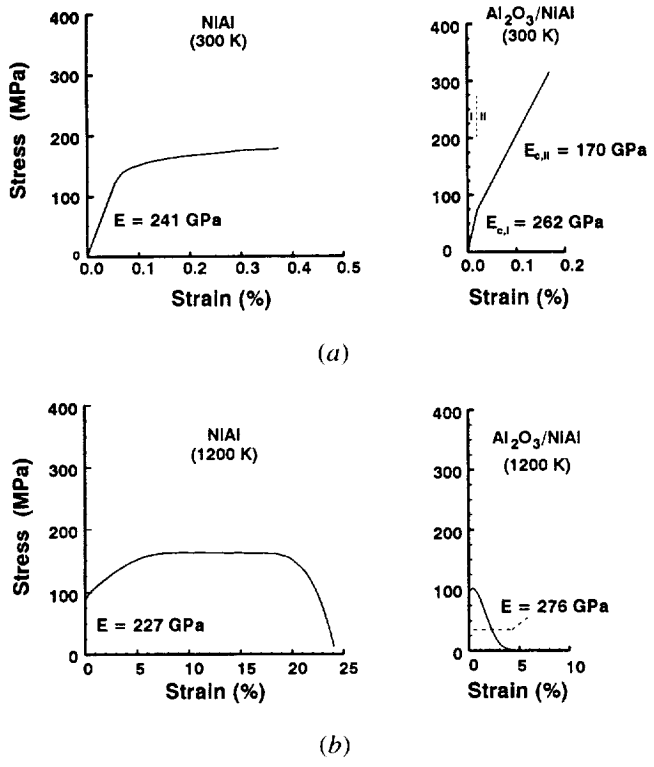

Fig. 5—Tensile response of NiAl and Al_2O_3/NiAl composite at (*a*) 300 and (*b*) 1200 K.

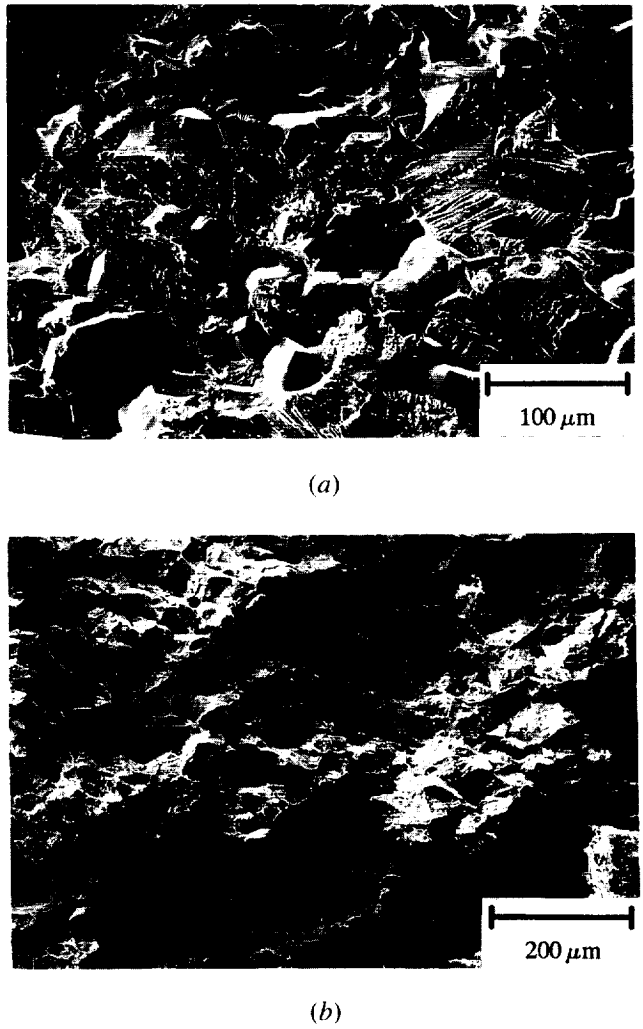

Fig. 6—Scanning electron micrographs of NiAl monolithic tensile fracture surfaces showing (*a*) intergranular fracture and transgranular cleavage at 300 K and (*b*) ductile fracture at 1200 K.

and impurity levels, powders from individual heats obtained for this study had a wide range of yield strengths ranging from about 120 to over 400 MPa. As mentioned previously, all properties reported here are from specimens fabricated from a single heat of low-strength material. At 1200 K, the elastic modulus was 227 GPa and the yield stress was approximately 70 MPa, with failure strains in excess of 20 pct. No AE events were noted before failure of the matrix-only specimens at room temperature (AE data for high-temperature tests cannot be obtained with the current experimental setup). Metallographic examinations of the tested specimens show that matrix cracking occurred only in the regions immediately adjacent to the final fracture sites. No matrix cracking was observed in specimens interrupted before failure. Scanning electron microscopy of transverse sections revealed the fracture mode at 300 K to be a combination of intergranular fracture and transgranular cleavage (Figure 6(a)), while at 1200 K (Figure 6(b)) a ductile fracture mode was observed.

2. *Powder-Cloth, Weakly Bonded Al_2O_3/NiAl Composites*

Representative stress-strain curves based on eight tensile tests for the PC processed Al_2O_3/NiAl composites tested at 300 and 1200 K are also shown in Figures 5(a) and (b), respectively, along with the monolithic results previously described. At 300 K, the PC processed Al_2O_3/NiAl composite exhibited two-stage tensile behavior, with the transition from stage I to stage II occurring at a composite strain ($\varepsilon_{c,I}$) of 0.028 pct; the corresponding composite stress at the transition was 73.6 MPa. The composite modulus in the initial stage ($E_{c,I}$ in Figure 5(a)) was 262 ± 43 GPa and the stage II modulus ($E_{c,II}$) was measured to be 170 ± 32 GPa. Actually, the stage II modulus was not constant but decreased with increasing strain. The value of $E_{c,II}$ ranged from 184 GPa at the onset of stage II to 163 GPa at failure. The average PC composite failure strain ($\varepsilon_{c,f}$) was 0.17 pct. In Figure 7, an Al_2O_3/NiAl composite tensile curve at 300 K is shown along with the associated AE data. Acoustic emissions began at the onset of the stage II behavior and occurred homogeneously throughout the specimen gage length for the entire stage II regime. The amplitude of the AE events ranged from 80 to 105 dB. Failure occurred catastrophically at the maximum load, with no measurable reduction in area of the gage section.

A typical high-temperature tensile curve, based on five tests of the weakly bonded composites, is also presented in Figure 5(b). This figure shows that the elevated temperature properties of the PC processed material are inferior to those at 300 K; further, both the composite strength (flow and fracture) and failure strain were less than that of the monolithic material. The average

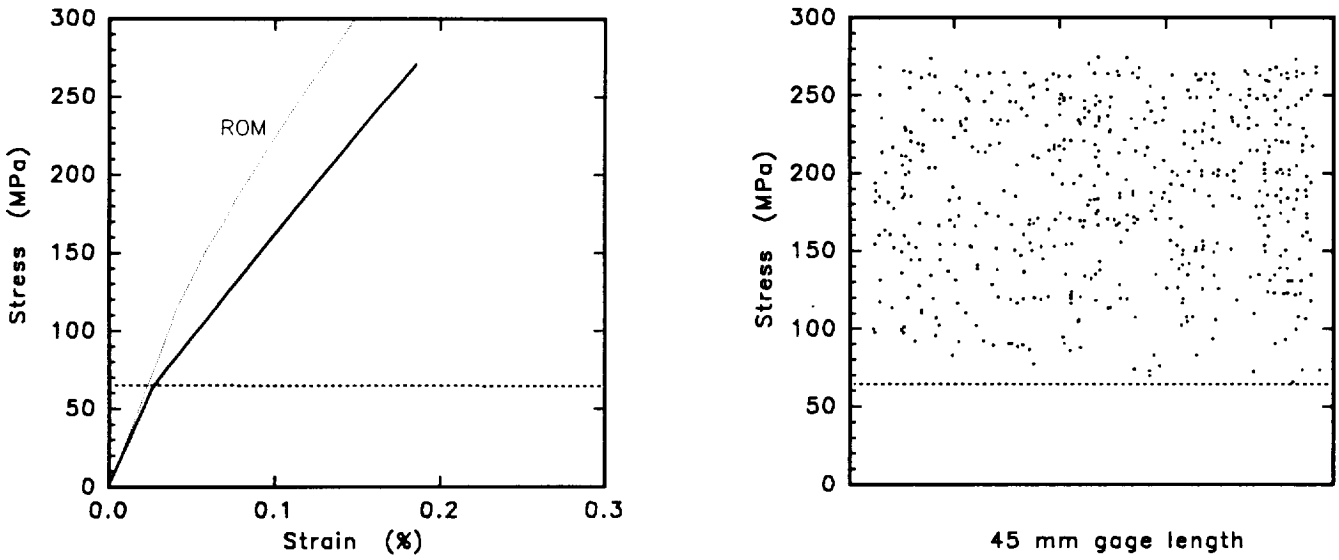

(*a*) (*b*)

Fig. 7—(*a*) Tensile response of weakly bonded Al_2O_3/NiAl composite at 300 K. (*b*) AE data collected during composite testing indicates that the first *in situ* fiber failures occurred at the onset of the stage II regime. Location of the AE events show that fiber failures occurred homogeneously throughout the gage section and eventually resulted in composite fracture.

Al_2O_3/NiAl modulus was 276 GPa, which is slightly higher than the monolithic. The modulus did not exhibit a measurable two-stage behavior, as was observed in the room temperature tests. The composite ultimate stress was 105 MPa and occurred at a strain of 0.038 pct. Catastrophic composite failure did not occur at the maximum load as in the 300 K tests. The tests were stopped when the stress dropped below 5 MPa after achieving an average total elongation of about 7 pct with a gage section reduction in area of 4.1 pct.

Scanning electron microscopy of the composite fracture surfaces are shown in Figure 8. The composite fracture mode differed from the monolithic in that both the 300 and 1200 K composite fracture surfaces were entirely intergranular fracture. This is in contrast to the monolithic, which was a mixture of intergranular fracture and transgranular cleavage at 300 K and ductile fracture at 1200 K.

Metallography of composite specimens tensile tested at 300 K showed numerous fiber failures throughout the gage length as well as transverse matrix cracks near the final fracture site. Because broken fibers were present in the untested material, fiber extractions were performed to better quantify any additional fiber fragmentation that may have occurred during the tensile test. The extracted fiber-size histogram for a weakly bonded composite tensile tested at 300 and 1200 K is shown in Figure 9. By comparing this figure to the fiber distribution of an as-fabricated specimen (Figure 3), it is clear that additional fragmentation of the fibers has occurred as a result of the tensile test because the number of long fibers has decreased. Figure 9 shows that fiber fragmentation during testing is more extensive at 1200 K (no fibers longer than 4 cm) as compared to 300 K.

Metallographic examinations showed no evidence of matrix cracking at either 300 or 1200 K in specimens interrupted prior to failure. The lack of matrix cracks prior to final failure and the occurrence of additional fiber fragmentation during tensile testing indicate that the AE events are associated with either fiber failures or possibly fiber debonding but not with matrix cracking, as is the case in some brittle-matrix composites. Scanning electron microscopy of the tested samples (Figure 8) shows fiber pullout in both the 300 and 1200 K tests. The average pullout length at 300 K was 500 μm compared to 120 μm at 1200 K.

IV. DISCUSSION

A. *Bond Strength*

The absence of a pronounced load drop after reaching the maximum load during fiber pushout of PC processed material is indicative of a purely mechanical interfacial bond with little or no chemical component.[21] This mechanical bond, equal to ~100 MPa at room temperature, arises from thermomechanical clamping of the fiber by the matrix during cooling from the processing temperature due to the higher CTE of the matrix and from mechanical interlocking of asperities on the fiber surface with the matrix. Conversely, the abrupt load drop in the binderless material pushout curves is evidence of a chemical bond (>280 MPa) between fiber and matrix. Once the chemical bond has been broken, the fiber can continue to slide at some load that is controlled by the clamping stress and interfacial friction. The formation of a strong bond between NiAl and Al_2O_3 in the binderless material is consistent with other observations in which strong bonding was measured in directionally solidified castings of NiAl containing Al_2O_3 fibers[31] (where no binders were present) and between bulk Al_2O_3 and NiAl plates subjected to hot pressing.[32]

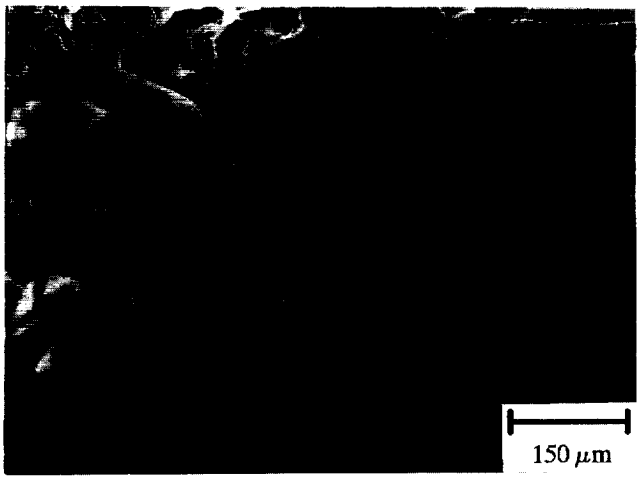

(*a*)

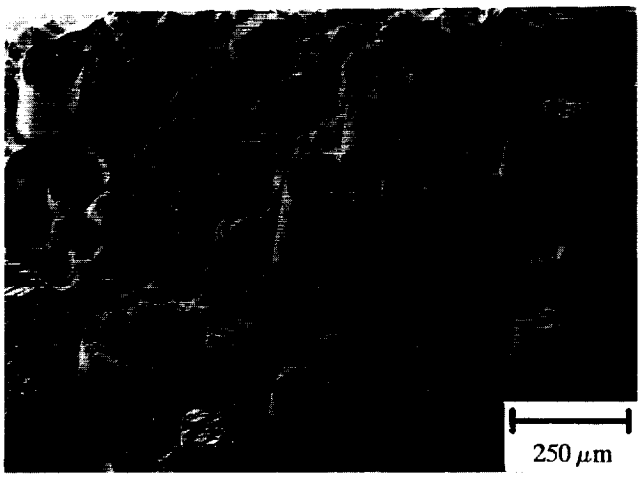

(*b*)

Fig. 8—Scanning electron micrographs of weakly bonded Al_2O_3/NiAl composite fracture surfaces tested in tension at (*a*) 300 and (*b*) 1200 K. At high temperature, the low fiber strengths resulted in fiber fracture rather than pullout resulting in greater pullout lengths at 300 K.

From these observations, one can conclude that the presence of binders inhibits bonding between the NiAl matrix and Al_2O_3 fibers. The actual mechanism(s) responsible for chemical bonding and the prevention of bonding by the binders is not well understood, however. Based on thermodynamic calculations, NiAl and Al_2O_3 are predicted to be mutually insoluble and nonreactive.[19] Metallography and EDS experiments detected no reaction products or diffusion. Strong bonding or chemical reaction is often associated with topological roughening of the alumina surface,[29,33,36] which is suspected to be a major contributor to the strength loss of Al_2O_3. However, observations of good bonding (~160 MPa) between Al_2O_3 and a Ni alloy in the absence of a chemical reaction or surface roughening has been noted.[27] Likewise, in the present study, no difference in fiber surface roughness or fiber tensile strengths were noted between strongly and weakly bonded specimens.

The PMMA and TEFLON were selected as the fiber and matrix binders, respectively, because 100 pct regeneration of their monomers is expected during pyrolytic depolymerization. It was thought that complete binder removal could be accomplished without charring or forming residues. However, recent work[34] has suggested that Al_2O_3 may act as a catalyst resulting in carbonization of the PMMA monomer during binder removal. This is consistent with the carbon residue observed on the fibers in PC processed composites. It has been consistently observed that the strength of the Al_2O_3 metal bond is strongly influenced by both the surface chemistry of the fiber[35] and the matrix composition.[36–39] Also, it is well established that the adherence of Al_2O_3 scales on NiAl formed during oxidation is dramatically affected by surface impurities.[1] It is reasonable to assume that the weak bonds that form in the PC processed materials are related to the presence of impurities from the binders that deposit onto on the fiber surfaces and thereby inhibit bonding. A more detailed study of fiber surface chemistry, fiber bonding, and fiber strength degradation is ongoing and is discussed in brief subsequently.

B. *Fiber Damage*

Metallography of longitudinal sections reveal that, as has been previously noted with other matrix materials, processing has resulted in fiber fractures. The fiber fractures in which matrix infiltrated between the fractured ends (Figure 2(a)) must have occurred prior to cooling from the consolidation temperature. The combination of high temperature and pressure allows the NiAl powders to infiltrate between the fractured segments. The fractures in which no matrix infiltration occurred (Figure 2(b)) could result from the compressive loading of the fibers due to the fiber-matrix CTE mismatch during cooling from the consolidation temperature. The compressive loading would also prevent subsequent matrix infiltration. It is also possible that the residual compressive loads on the fibers, which were generated during cooling, could promote twinning. The twinned regions would be weak points subject to failure. However, no twinning was observed in any fibers examined in this study. This is not conclusive evidence against twinning, however, because twins in sapphire are often difficult to observe. It is also possible that the uninfiltrated cracks were artifacts generated during metallographic preparation. Nondestructive X-ray techniques were employed on as-fabricated plates in an attempt to resolve this issue; unfortunately, the resolution of the X-ray images was insufficient to confirm or dispute the existence of the fine cracks in unpolished samples. If these cracks were formed during grinding or polishing, then they should be observed in all composites regardless of matrix composition, provided that the grinding and polishing procedures were identical. Comparison with other systems under investigation at NASA has revealed that fewer compression cracks are observed in Al_2O_3/FeAl matrix composites compared to Al_2O_3/NiAl and are almost nonexistent in Al_2O_3/FeCrAlY composites.[40] All composites were metallographically prepared by identical procedures, thus strongly suggesting that the uninfiltrated cracks are a consequence of the composite system and are not an artifact.

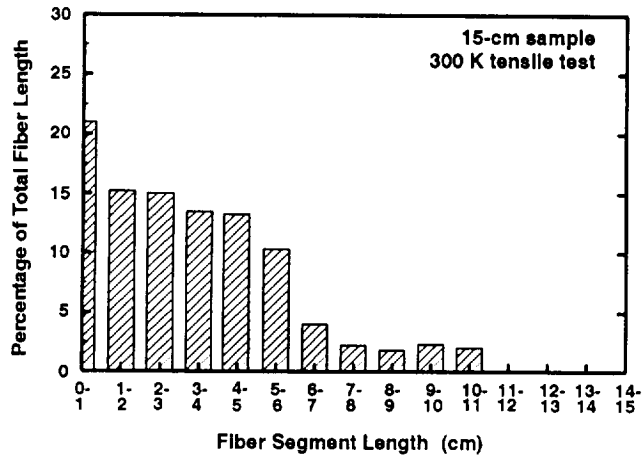

(*a*)

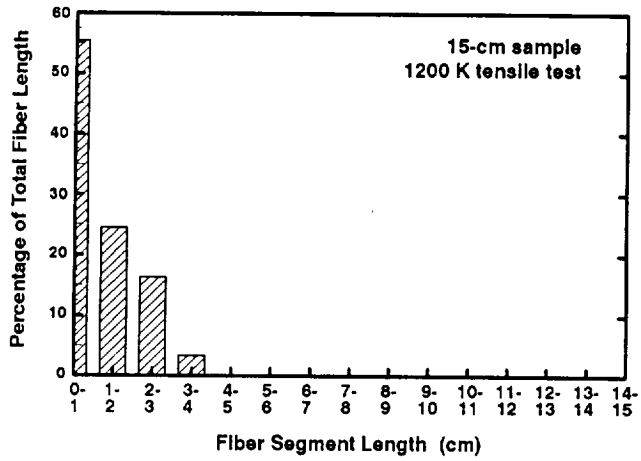

(*b*)

Fig. 9—Length distribution of fibers extracted from composite specimens tensile tested at (*a*) 300 and (*b*) 1200 K. Compared to the as-fabricated distribution (Fig. 3), some additional fiber fragmentation is observed after the 300 K test and extensive fragmentation is observed after testing at 1200 K.

The extraction studies clearly show that no full-length fibers survive the consolidation process either by the PC or binderless technique. The histogram of fiber lengths of a 5 × 15 cm plate in Figure 3 clearly illustrates the degree of fragmentation that occurs during processing of PC composites. As previously mentioned, extracted fibers had severe strength degradation and surface ridging. While the presence of binders changes the bond character, it has no effect on fiber-matrix reaction, surface ridging, or fiber degradation. In any event, these mechanisms can not in themselves explain the fragmentation. Composites have been made[41] using a Ni-32.5Al-20Fe matrix reinforced with 30 vol pct Al_2O_3 fibers, in which both ridging and strength loss were observed but no fiber fragmentation occurred during processing. While fiber strength loss undoubtedly plays a role, so do the mechanical properties and perhaps the chemistry of the matrix, which in the case of Reference 41 were not dramatically different from those of NiAl. These results also show that the fiber extraction process itself is not responsible for the fiber fractures because full-length fibers were extracted from the alloyed matrix in every specimen examined.

Strength degradation of the Al_2O_3 fibers during processing is a major concern and has been the topic of recent investigations.[26,28,42] Possible mechanisms for the strength loss include fiber-matrix reaction, reaction with binders or impurities, residual stresses, and damage induced during handling or consolidation.[26] The importance of matrix chemistry has been highlighted by Draper *et al.*,[28] who examined Al_2O_3 fibers sputtered-coated with NiAl in an attempt to separate fiber damage from chemical interactions and from mechanical damage, as may be experienced during hot-pressing. In the as-coated condition, the Al_2O_3 fibers had a tensile strength of 2420 MPa, which was only slightly less than the uncoated strengths. After subjecting the coated fibers to an annealing treatment that simulated the NiAl composite fabrication cycle, the fiber tensile strength decreased to 1200 MPa. A similar thermal treatment on uncoated fibers had no effect on the fiber strengths. It is therefore clear that some interaction does occur between NiAl and Al_2O_3 that degrades the strengths of the fibers. While the ridging phenomena may play a role, the mechanism of the fiber strength loss is still unclear. Simple stress-intensity calculations[26] based on the height of the ridges suggest that the ridges in themselves cannot account for the magnitude of the strength loss observed. Because all of the proposed mechanisms are interrelated to some degree, their individual effects were hard to separate. However, it was concluded that fiber-matrix reactions were the dominant mechanism for the strength loss. In this context, fiber-matrix reaction is used in a generic sense to describe some sort of fiber-matrix interaction and does not imply the formation of observable second phases.

C. *Tensile Deformation*

An important question concerning further discussions is what effect does the discontinuous nature of the reinforcing fibers have on composite properties. An obvious concern is how effective the fibers are in transferring load when compared to the original continuous state. Based on the measured extracted fiber lengths and using models developed for discontinuous composites, the composite containing fragmented fibers is found to have 96 pct the strengthening capability of a composite with continuous fibers. Based on these analysis, no significant deviation from rule of mixtures (ROM)-predictions for modulus or flow strength should result due to reduced load-carrying capacity of the discontinuous fibers. However, the modulus can be strongly dependent on the geometric arrangement of the fibers.[43] Achieving a ROM modulus requires overlapping between adjacent fiber ends. If fiber cracks were localized in one plane, then the applied load would be carried primarily by the matrix in the regions of nonoverlapping fibers. Optical metallography has shown this not to be the case, thus no reduction in modulus is expected. While these discontinuous composites are similar to a continuous composite in terms of load-carrying capacity, the presence of embedded fiber ends can have significant influence on the composite

fracture behavior. A number of models and experimental studies[44,45] have attempted to analyze this situation in terms of stress concentrations at the fiber ends. Even though the details vary, all studies confirm that the local stress concentrations will reduce the fracture stress of the discontinuous composite by promoting matrix cracking at the fiber ends. However, the same models also predict that the effect of short fibers in reducing the fracture stress is diminished for aspect ratios greater than about 50. Because the average aspect ratio of the Al_2O_3/NiAl composites is much greater than 150, it appears that the fiber fragmentation may not significantly reduce the composite fracture stress.

1. *Room temperature*

The two-stage tensile behavior shown in Figure 5(a) for Al_2O_3/NiAl at 300 K has been observed in a wide range of composite materials.[46,47,48] The composite strain, averaged for all specimens, at the onset of stage II (where the first fiber failures were noted by AE) was 2.81×10^{-4}, which corresponds to a fiber stress of 126 MPa. This simple calculation assumes isostrain conditions with a fiber elastic modulus of 450 GPa and assumes the as-fabricated fiber stress was zero. In comparison, Figure 4 shows that the weakest extracted fibers had a fracture strength of 760 MPa, which is much stronger than the *in situ* fibers based on the AE data. Low *in situ* fiber strengths are possibly attributable to the poor bend strength of the damaged fibers. As-received fibers could be bent around a very small radius, whereas extracted fibers could tolerate only minuscule bending. Consequently, in the composite, imperfect fiber alignment with respect to the composite longitudinal axis will lead to a bending stress on the fiber during the tensile test and hence lower the fiber fracture strength. The reason the fiber failures begin at the onset of stage II behavior is unknown and is difficult to speculate on since it is not yet clear what is responsible for the change in composite compliance.

The observed inelastic deformation at the end of stage I in Figure 5(a) can result either from matrix plasticity or damage. Damage can be in many forms, such as matrix or fiber cracking or interfacial debonding. Damage can be detected by examining metallographic specimens taken from a specimen loaded into stage II and looking for evidence of matrix or fiber cracking. Because the metallographic results of interrupted tests failed to reveal any matrix cracking even after loading the specimen well into the stage II regime, there is no evidence that matrix cracking is the mechanism responsible for the inelastic behavior. As for fiber fractures, the first fiber failure (in addition to those which occurred during processing) occurred at the onset of stage II, as observed in Figure 7. This was true for all specimens (weakly bonded) tested in this program. Because a single fiber failure is incapable of changing the composite modulus to the extent observed, it follows that the fiber failure is a *result* of the inelastic behavior and not the cause.

Analytical modeling was performed in an attempt to understand the reasons for the bilinear response. The material properties used in those calculations are given in Table II. The onset of stage II in some systems has been found to correspond to the stress at which the matrix begins to deform plastically[47,48] or when tensile failure of the matrix at the ends of fragmented fibers occurs.[49] In most composite systems, the average stress in the matrix at the onset of stage II is usually less than the yield stress of the monolithic material due to the presence of residual stresses. In the present system, assuming isostrain conditions, the average matrix stress at the onset of stage II behavior would be only 68 MPa (E_m = 241 GPa, $\varepsilon_1 = 2.81 \times 10^{-4}$) if it is assumed that the matrix is stress free at the onset of the tensile test. Thus, the composite matrix yields at about 50 MPa less than the yield stress of the monolithic NiAl samples (Figure 5(a)). This could be interpreted to mean that the matrix has remained elastic but accumulated approximately 50 MPa of residual tensile stress during cool-down. However, experimental evidence suggests that such a straight-forward explanation is unsatisfactory. Transmission electron microscopy of as-processed P-C composites has shown that extensive matrix yielding occurs during cooldown from the consolidation temperature.[50] Thus in this system, the onset of stage II cannot be related simply to the onset of matrix plasticity because extensive plasticity is present in the as-fabricated condition. Also, neutron diffraction measurements[17,51] have shown that the matrix stress after fabrication is on the order of 200 MPa rather than 50 MPa. One possibility under investigation is that some relaxation of the residual stresses occurs after fabrication due to creep mechanisms, fiber-matrix slippage, etc. In this case, some elastic matrix loading could occur during the subsequent tensile test before matrix plasticity was resumed and hence the composite would exhibit the two-stage behavior observed.

Debonding of the fiber from the matrix is another possible explanation for the change in composite compliance. If fiber debonding occurs, then load cannot be effectively transferred to the fibers from the matrix and hence the stiffness of the composite will decrease. Debonding has also been linked to AE events and thus is consistent with the observation of AE events occurring at the beginning of stage II. However, the amplitude of AE events associated with matrix cracking and debonding is generally around 40 to 80 dB. Amplitudes greater than 80 dB, as were measured in the Al_2O_3/NiAl composites (Section III–D–2), are more typical of fiber breakage.[52] Also, the dramatic decrease in composite compliance that occurs at the onset of stage II cannot be attributed to a single debonding event (or a single-fiber failure if the AE events are associated with fiber failures). In addition, close examination of composite fracture surfaces fails to show any evidence of debonded interfaces. Finally, fiber pushout experiments showed that the interfacial bond strengths were the same before and after tensile testing. Although it is possible that too few fibers were tested for interfacial strength to say conclusively that no fibers were debonded, these results taken along with the metallography and AE data suggest that fiber debonding is not the primary mechanism for the change in compliance.

From initial concentric-cylinder model calculations, it became clear that the predicted residual stress state in the composite was very sensitive to the assumed stress-free temperature (T_{sf}). The stress-free temperature is where matrix (and fiber) stresses begin to increase during cooling from the consolidation temperature. Because T_{sf} is

affected by many variables, it was not possible to estimate *a priori* a value for T_{sf}. Since no experimental data of T_{sf} was available, it became necessary to choose a T_{sf} that made physical sense and was consistent with the experimental observations of tensile properties (Section III–D), interfacial dislocation morphology after cooldown[50] (an indication of the extent of plasticity), and composite residual stresses measured by neutron diffraction. Because a "first-principal" calculation was not possible due to incomplete data, the modeling results were utilized more as an aid to understanding rather than as a predictive tool.

As a starting point, a T_{sf} was chosen such that the predicted matrix and fiber stresses would be similar to those measured by neutron diffraction. Using 850 K for T_{sf} resulted in the stress state depicted in Figure 10(a), where the average matrix axial stress was 200 MPa (tensile) and the fiber was under a compressive stress of 445 MPa. This compares closely with the neutron diffraction results, which measured a matrix stress of 240 MPa and fiber stress of −445 MPa. Transmission electron microscopy (TEM) of as-fabricated specimens showed that extensive dislocation generation occurs at the vicinity of the fiber-matrix interface during cooling from the processing temperature.[50] Also, the dislocation density away from the fiber was higher than as-fabricated monolithic NiAl, indicating that the entire matrix cross section had undergone some plastic deformation. This is consistent with the model prediction shown in Figure 10(b), which shows nonzero plastic strain throughout the matrix. Both the experimental observations and the model indicate the occurrence of the greatest strain near the interface, as would be expected. The assumed T_{sf} of 850 K is also consistent with the TEM study, where it was deduced based on the observed dislocation morphology, that the matrix was plastically deformed in the intermediate temperature range of 700 to 900 K. In Figure 11(a), the stresses in the individual components are shown during a simulated tensile test assuming a T_{sf} of 850 K. At the end of stage I (ε = 0.028 pct), where the first fiber failures occur, the model predicts the fibers still to be in compression. This is not inconsistent with the premise of fiber fractures occurring at this strain since the fibers are as likely to fail due to bending as to tensile stresses. One other interesting note is that at the average composite fracture strain (0.17 pct), the stress in the matrix, fiber, and composite are all roughly equal to 270 MPa, which is the measured macroscopic composite fracture stress. The significance of this observation, if any, is unknown.

Although the composite stresses and dislocation structure can be rationalized assuming a T_{sf} of 850 K, this choice of T_{sf} does result in inconsistencies with the predicted tensile response. In particular, Figure 11(b) shows computer simulations of macroscopic tensile behavior of as-fabricated specimens assuming various T_{sf} values. The key feature of Figure 11(b) is that the predicted tensile curve for T_{sf} values greater than 580 K are essentially linear over the entire test. In order to obtain a bilinear response, which is similar to the experimentally obtained tensile curve (Figure 5(a)), requires T_{sf} to be approximately 450 K. With this lower value of T_{sf}, matrix plasticity during cooldown is confined to a region adjacent

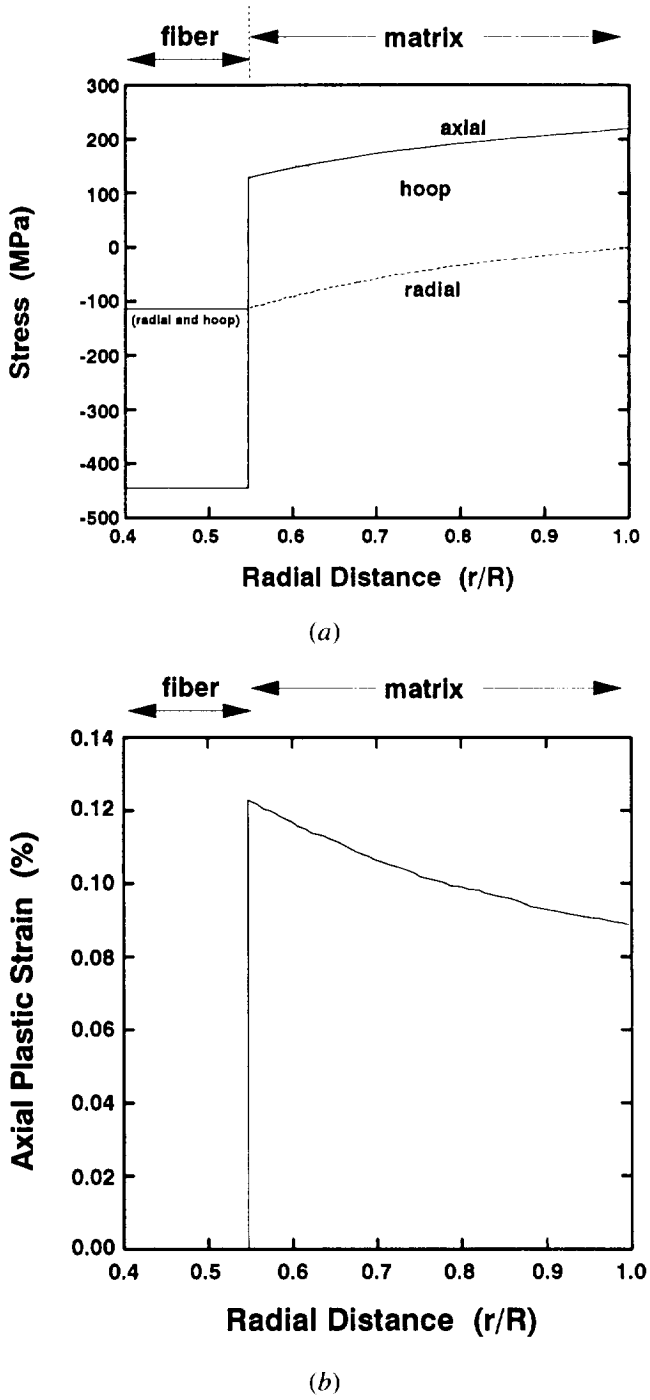

Fig. 10—(*a*) Residual stress state after fabrication of a Al_2O_3/NiAl composite assuming a stress-free temperature of 850 K. (*b*) Predicted matrix plasticity resulting from the residual stresses. *r* is the radial distance from the center of the fiber, and *R* is the radius of the concentric cylinder used in the model.

to the fiber-matrix interface. For this condition, the growth of the plastic zone in the matrix is associated with the stage I region of the tensile curve; stage II behavior is observed after plasticity has engulfed the entire matrix. It is difficult to envision a mechanism that could explain such a low, stress-free temperature. It is clear that the model is not yet sophisticated enough to account for all the factors that operate during composite processing and

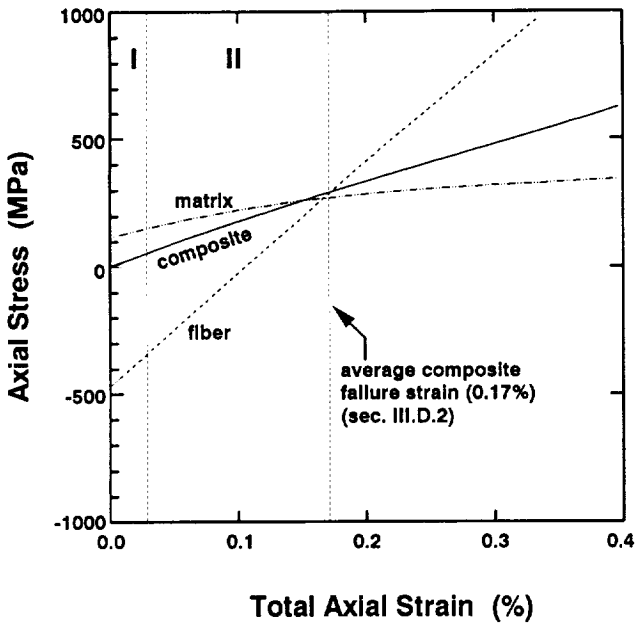

(*a*)

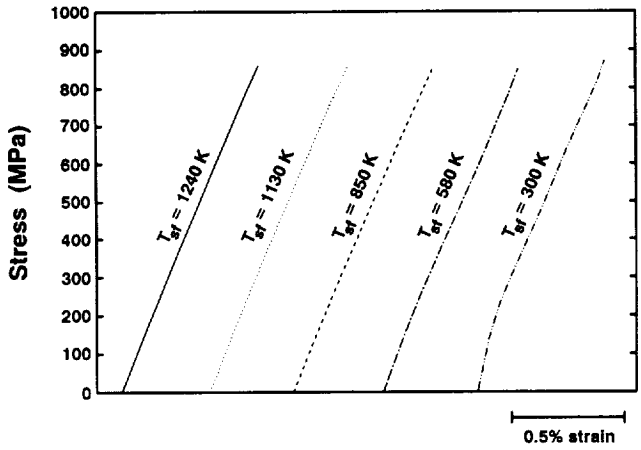

(*b*)

Fig. 11—Concentric cylinder model predictions of (*a*) various component stresses as a function of strain during a tensile test assuming a stress-free temperature (T_{sf}) of 850 K and (*b*) macroscopic composite behavior under tensile loading, assuming various values for T_{sf} during cooling.

subsequent mechanical testing. Continued refinement of the model to include other factors, such as matrix creep, are underway.

The ROM predicts a room-temperature composite modulus of 293 GPa (assuming a fiber modulus of 450 GPa and a matrix modulus of 241 GPa from Section II–D–1). The ROM overestimates the composite modulus, which was measured to be 262 GPa. In addition to the invalid assumption of the matrix being elastic in the stage I regime, deviations from predicted ROM values can occur when the fibers are not equally strong, poorly aligned, weakly bonded, or inhomogeneously distributed throughout the matrix. Because most, if not all, of these exceptions are present in these composites, it is not unexpected to see deviations from the predicted ROM modulus.

As a baseline, a simple ROM prediction for failure stress of a continuous-fiber composite (σ_c^*) with perfect bonding and a fiber failure strain that is less than the matrix can be predicted using the fracture stress of the fiber and the stress in the matrix at the breaking strain of the fiber. Using the minimum extracted fiber strengths results in a predicted Al_2O_3/NiAl fracture stress of 318 MPa, which overestimates the actual fracture stress (270 MPa). One reason for this is that the AE data clearly show that fiber fractures occur at stress much below the extracted values used in these calculations; AE data indicate that fiber fractures occur as low as 126 MPa. Using this value for fiber strength yields a continuous-fiber composite fracture stress of 81 MPa at 300 K, which now underestimates the actual stress.

Another factor that may influence failure stress is the residual stress in the composite after consolidation. The model predicts residual tensile stresses in the matrix and compressive stresses in the fiber. Thus, the effective strength of the matrix is lowered and the effective strength of the fiber is raised. The consequence of these residual stresses depends on whether the composite failure is controlled by fiber or matrix failure, and a model has been proposed to account for this.[51] It was concluded that when fibers control failure (*i.e.*, the fibers reach their failure strain before the matrix), the residual stresses should have no effect on composite failure stress. Conversely, when matrix failure occurs before the fibers, then tensile matrix residual stresses act to reduce the composite stress (or matrix cracking stress) below that predicted by ROM. Because the Al_2O_3 fibers fail before the NiAl matrix, this model predicts that the residual stresses do not account for the low composite strengths.

All of these models assume that composite failure is controlled by first fiber fracture. The AE data clearly shows that multiple fiber fractures occur prior to composite failure. This is supported by computer simulations of composites with V_f greater than 15 pct, in which it was observed that fiber failures occur at separate regions before matrix fracture starts.[53] Curtin[54] developed a model for composite failure, again assuming that fiber fracture controls composite failure but also allowed for multiple fractures, incorporated the statistical nature of fiber strength, and included gage length effects. The predicted fracture stress is *independent* of residual stresses in the composite. It is assumed that the fibers carry the majority of the load after matrix yielding. Using extracted fiber strengths, the model predicts a 300 K composite failure stress of 535 MPa and a failure strain of 0.004. The actual values are $\sigma_c^* = 270$ MPa and $\varepsilon_c^* = 0.0018$. Again, AE data reveals that fiber fractures occur at stresses significantly below those in the extracted condition and must be accounted for when predicting composite fracture stress. The lowest extracted fiber tensile strength was 760 MPa, while AE detected fiber failures at strains that correspond to fiber strengths of 126 MPa. If the extracted fiber stress distribution is reduced by 630 MPa (to roughly estimate the *in situ* fiber strength distribution), then the calculated composite fracture stress is 288 MPa and the failure strain is 0.0018, which closely agrees with the observed values. Therefore, failure in

Al_2O_3/NiAl is not controlled by the onset of fiber failure. However, cumulative fiber failures eventually produce sufficient stress concentrations to initiate failure in the matrix. Also, the primary reason for the lower than expected composite strengths is due to low *in situ* fiber strengths.

2. *High temperature*

The high-temperature behavior of the weakly bonded Al_2O_3/NiAl composites shown in Figure 5 differed from the low-temperature results in that the load increased linearly to a maximum followed by a gradual load drop rather than the bilinear loading to fracture observed at room temperature. Due to the lack of chemical bonding, the interface strength in this composite arises from mechanical locking and compressive radial stresses that are generated during cooling. It has been a concern that bonding, and hence strengthening, would be lost at high temperatures where the compressive radial stresses would be relieved. A high-temperature modulus was calculated using the simple ROM calculation. Using the temperature-compensated values of matrix and fiber modulus resulted in a predicted composite modulus of 294 GPa, which, like the room-temperature predictions, slightly overestimates the measured composite modulus of 276 GPa. However, since the ROM predictions do not significantly deviate from the measured values of modulus, it must be assumed that sufficient bonding remains at this temperature to allow strengthening from the fibers. The fact that the fiber pullout lengths were shorter at 1200 K is also consistent with the presence of some bonding that allowed for fiber loading and subsequent failure rather than fiber pullout. High-temperature pushout testing was attempted on these composites to quantify the bond strength but was inconclusive because matrix yielding occurred concurrently with fiber pushout, making quantitative measurements of the bond strength difficult. Issues of thermal behavior of bonding and cracking are the subject of another study.[55]

While no AE data could be obtained at high temperature, the extracted fiber lengths after high-temperature testing (Figure 9(b)) show that extensive fiber failure occurs during tensile testing. What was not determined was whether these fiber failures occurred prior to the maximum stress or developed during the extensive deformation following this peak load. However, in light of the low fracture stress of the composite, the degradation in fiber strength (both due to processing and the increase in temperature) is undoubtably the most serious concern for Al_2O_3/NiAl. A major motivation for developing Al_2O_3/NiAl was that the properties of NiAl composites appeared attractive at high temperatures based on ROM predictions of strength. For example, if as-received fiber properties are assumed, the fracture stress of Al_2O_3/NiAl at 1200 K is predicted to be 782 MPa with a failure strain of 0.3 pct. It was not possible to account for fiber damage and accurately predict strengths at 1200 K, as was done at room temperature, because the *in situ* fiber properties could not be estimated (no AE data to estimate fiber failure stresses), and the high-temperature pushout data were difficult to interpret. However, using the extracted properties in Figure 4 and assuming a perfect bond, results in a predicted strength of only 331 MPa at 1200 K, which, even on a density compensated basis, is not competitive with superalloys. In the actual composite, where poor bonding is present in addition to the degraded fiber properties (due to temperature effects, matrix reaction, and fiber fragmentation), the measured maximum composite stress was only 105 MPa at 1200 K.

V. SUMMARY

1. A weak, frictional interfacial bond (~100 MPa) formed in Al_2O_3/NiAl composites fabricated using the PC technique. Conversely, a strong chemical bond (~280 MPa) formed in composites made without fugitive binders.
2. Weakly bonded Al_2O_3/NiAl composites could be fabricated without the formation of matrix cracks, although extensive fiber fractures were observed. Fiber fractures were also observed in the strongly bonded composites, as was matrix cracking in large specimens.
3. A significant reduction in fiber strength was measured in fibers extracted from as-fabricated NiAl composites. A drop in fiber strength was also observed at high test temperatures for both as-received and extracted fibers. Fiber surface attack was observed in extracted fibers in the form of ridges that corresponded to the grain boundaries of the NiAl matrix material.
4. The tensile responses of weakly bonded composites showed bilinear behavior at room temperature but not at 1200 K. At both temperatures, the composite strengths were below ROM predictions. Composite failure strain at 300 K was 0.17 pct and was achieved through extensive fiber pullout. At 1200 K, as much as 30 pct elongation was observed with measurable matrix plasticity and less fiber pullout than observed at 300 K.
5. Fiber failures began at the onset of the stage II regime and occurred homogeneously throughout the gage length for the remainder of the test. No matrix cracking was observed prior to final failure of the specimen. Fiber failures were noted by AE and by examining the extracted fiber size distributions.

VI. CONCLUSIONS

The same dilemma that was found in earlier studies of metal matrix composites also exists in NiAl matrices. That is, the primary technical obstacle to the development of these composites is fiber strength degradation. The observation that some NiAl-derivative matrices do not result in fiber degradation offers some hope that through matrix alloying, it may be possible to tailor the matrix composition in such a way as to achieve a useful composite system. In particular, from the experimental work in this study of strongly and weakly bonded Al_2O_3/NiAl composites, the following conclusions are drawn.

1. The bond strength between NiAl and Al_2O_3 is inherently strong. The presence of surface impurities (such as the binders used in the PC technique) inhibit the formation of this bond.
2. A weak fiber-matrix bond prevents matrix cracking

during fabrication. The tendency for cracking in strongly bonded composites appears to be greater than in the weakly bonded ones; however, further tests are required for confirmation.

3. A degradation of fiber strength results from high-temperature exposure to NiAl (such as encountered during fabrication or service). Both the mechanism for the fiber degradation and a solution to the problem are as yet unknown, although changes in matrix composition can influence both fiber fracture during fabrication and the degree of fiber-matrix reaction.
4. Primarily because of the fiber strength degradation, the properties of Al_2O_3/NiAl composites fall well below expectations and, therefore, the composite is unsuitable for structural applications.

REFERENCES

1. R.D. Noebe, R.R. Bowman, and M.V. Nathal: *Int. Met. Rev.*, 1993, vol. 38, pp. 193-232.
2. R. Darolia: *J. Met.*, 1991, vol. 43, pp. 44-49.
3. S.C. Huang, R.D. Field, and D.D. Krueger: *Metall. Trans. A*, 1990, vol. 21A, pp. 959-70.
4. P.R. Subramanian, M.G. Mendiratta, D.B. Miracle, and D.M. Dimiduk: *Intermetallic Matrix Composites*, Materials Research Society Symposia Proceedings, D.L. Anton, P.L. Martin, D.B. Miracle, and R. McMeeking, eds., MRS, Pittsburgh, PA, 1990, vol. 194, pp. 147-54.
5. J.L. Walter and H.E. Cline: *Metall. Trans.*, 1970, vol. 1, pp. 1221-29.
6. J.D. Whittenberger, R.K. Viswanadham, S.K. Mannan, and B. Sprissler: *J. Mater. Sci.*, 1990, vol. 25, pp. 35-44.
7. J.D. Whittenberger, E. Arzt, and M.J. Luton: *Scripta Metall. Mater.*, 1992, vol. 26, pp. 1925-30.
8. S.M. Barinov and V. Yu. Evdokimov: *Acta Metall. Mater.*, 1993, vol. 41, pp. 801-04.
9. K.S. Kumar, S.K. Mannan, and R.K. Viswanadham: *Acta Metall. Mater.*, 1992, vol. 40, pp. 1201-22.
10. S. Nourbakhsh, O. Sahin, W.H. Rhee, and H. Margolin: *Metall. Trans. A*, 1991, vol. 22A, pp. 3059-64.
11. R.R. Bowman: *Intermetallic Matrix Composites II*, Materials Research Society Symposia Proceedings, D.B. Miracle, D.L. Anton, and J.A. Graves, eds., MRS, Pittsburgh, PA, 1992, vol. 273, pp. 145-55.
12. D.L. Anton and D.M. Shah: *Intermetallic Matrix Composites II*, Materials Research Society Symposia Proceedings, D.B. Miracle, D.L. Anton, and J.A. Graves, eds., MRS, Pittsburgh, PA, 1992, vol. 273, pp. 157-64.
13. S.M. Jeng, J.-M. Yang, and R.A. Amato: *Intermetallic Matrix Composites II*, Materials Research Society Symposia Proceedings, D.B. Miracle, D.L. Anton, and J.A. Graves, eds., MRS, Pittsburgh, PA, 1992, vol. 273, pp. 217-25.
14. H.R. Gray and C.A. Ginty: *Proc. 5th Annual HITEMP Review*, NASA, Cleveland, OH, No. CP-10104, 1992, pp. 1-25.
15. R.W. Clark and J.D. Whittenberger: in *Thermal Expansion 8*, T.A. Hahn, ed., Plenum Press, New York, NY, 1984, pp. 189-96.
16. S. Reuss and H. Vehoff: *Scripta Metall. Mater.*, 1990, vol. 24, pp. 1021-26.
17. A. Saigal and D.S. Kupperman: *Scripta Metall. Mater.*, 1991, vol. 25, pp. 2547-52.
18. C. Calow and A. Moore: *J. Mater. Sci.*, 1972, vol. 7, pp. 543-58.
19. A.K. Misra: NASA Contractor Report No. CR-4141, 1988.
20. J.W. Pickens, R.D. Noebe, G.K. Watson, P.K. Brindley, and S.L. Draper: NASA Technical Memorandum No. TM-102060, 1989.
21. J.I. Eldridge, R.T. Bhatt, and J.D. Kiser: NASA Technical Memorandum No. TM-103739, 1991.
22. W. Weibull: *J. Appl. Mech.*, 1951, vol. 18, pp. 293-97.
23. B. Bergmen: *J. Mater. Sci. Lett.*, 1984, vol. 3, p. 689.
24. J.D. Sullivan and P.H. Lauzon: *J. Mater. Sci. Lett.*, 1986, vol. 5, pp. 1245-47.
25. S. van der Zwaag: *J. Testing Eval.*, 1989, vol. 17, pp. 292-98.
26. S.L. Draper and I.E. Locci: *J. Mater. Res.*, 1994, vol. 9, pp. 1397-1411.
27. L.J. Westfall: NASA Technical Memorandum No. TM X-3333, 1976.
28. S.L. Draper, J.I. Eldridge, and I.E. Locci: *Proc. 5th Annual HITEMP Review*, 1992 NASA, Cleveland, OH, No. CP-10104, pp. 17/1-17/13.
29. I.E. Reimanis: *Acta Metall. Mater.*, 1992, vol. 40, Suppl., pp. S67-S74.
30. S.L. Draper, D.J. Gaydosh, and A. Chulya: *Proc. of the 4th Annual HITEMP Review*, NASA, Cleveland, OH, No. CP-10082, 1991, pp. 42/1-42/14.
31. S.N. Tewari, R. Asthana, and R.D. Neobe: *Metall. Trans. A*, 1993, vol. 24A, pp. 2119-25.
32. R.D. Noebe and R.R. Bowman: NASA Lewis Research Center, Cleveland, OH, unpublished research, 1989.
33. J.E. Ritter, Jr. and M.S. Burton: *Trans. AIME*, 1967, vol. 239, pp. 21-26.
34. G.W. Watson: NASA Lewis Research Center, Cleveland, OH, unpublished research, 1993.
35. S.V. Pepper: *J. Appl. Phys.*, 1976, vol. 47, pp. 801-08.
36. W.H. Sutton and E. Feingold: *Mater. Sci. Res.*, 1966, vol. 3, pp. 577-611.
37. R.D. Monahan and J.W. Halloran: *J. Am. Ceram. Soc.*, 1979, vol. 62 (11-12), p. 564.
38. R.A. Page, J.E. Hack, R. Sherman, and G.R. Leverant: *Metall. Trans. A*, 1984, vol. 15A, pp. 1397-405.
39. R.L. Mehan and M.J. Noone: in *Composite Materials*, Academic Press, Inc., New York, NY, 1974, vol. 4, pp. 159-227.
40. Sue Draper: NASA Lewis Research Center, Cleveland, OH, private communication, 1993.
41. R.R. Bowman, I.E. Locci, and D.F. Lahrman: NASA Lewis Research Center, Cleveland, OH, and GE Aircraft Engines, Cincinnati, OH, unpublished research, 1993.
42. R.E. Tressler, S.A. Newcomb, and A. Sayir: *Proc. of the 5th Annual HITEMP Review*, NASA, Cleveland, OH, No. CP-10104, 1992, pp. 19/1-19/16.
43. J.-M. Berthelot, A. Cupcic, and K.A. Brou: *J. Comp. Mater.*, 1993, vol. 27, pp. 1391-1425.
44. S. Ochiai and K. Osamura: *Z. Metallkd.*, 1990, vol. 81, pp. 452-56.
45. Y. Termonia: *J. Mater. Sci.*, 1990, vol. 25, pp. 4644-53.
46. B. Lerch: NASA Technical Memorandum No. TM-103760, 1991.
47. P. Brindley, S. Draper, J. Eldridge, M. Nathal, and S. Arnold: *Metall. Trans. A*, 1992, vol. 23A, pp. 2527-40.
48. S. Nourbakhsh, W. Rhee, O. Sahin, and H. Margolin: *Mater. Sci. Eng.*, 1992, vol. A153, pp. 619-27.
49. Y. Termonia: *J. Mater. Sci.*, 1992, vol. 27, pp. 4878-82.
50. L. Wang, R.J. Arsenault, and Randy Bowman: University of Maryland, College Park, MD, and NASA Lewis Research Center, Cleveland, OH, unpublished research, 1993.
51. P.K. Wright, M.D. Sensmeier, D.S. Kupperman, and H.N.G. Wadley: NASA Contractor Report No. CR-191191, 1993.
52. M. Madhukar and J. Awerbuch: *Composite Materials: Testing and Design*, ASTM STP 893, ASTM, Philadelphia, PA, 1986, pp. 337-55.
53. M. Murat, M. Anholt, and H. Wagner: *J. Mater. Res.*, 1992, vol. 7, pp. 3120-31.
54. W.A. Curtin: *Composites*, 1993, vol. 24, pp. 98-102.
55. R.R. Bowman, A.K. Misra, and S.M. Arnold: NASA Lewis Research Center, unpublished research, 1994.